Structural and Optical Properties of (Zn,Mn)O Thin Films Prepared by Atomic Layer Deposition

Article *in* Journal of Vacuum Science & Technology A Vacuum Surfaces and Films · June 2020

DOI: 10.1116/6.0000141

3 authors:

Amirhossein Ghods
Missouri University of Science and Technology
28 PUBLICATIONS **80** CITATIONS
SEE PROFILE

Chuanle Zhou
Northwestern University
45 PUBLICATIONS **154** CITATIONS
SEE PROFILE

Ian Ferguson
Kennesaw State University
435 PUBLICATIONS **5,676** CITATIONS
SEE PROFILE

Structural and Optical Properties of (Zn,Mn)O Thin Films Prepared by Atomic Layer Deposition

Running title: ALD-ZnMnO Thin Films Growth and Characterization

Running Authors: Ghods et al.

Amirhossein Ghods [1], Chuanle Zhou [1], and Ian T. Ferguson [1,2,a)]

[1]Electrical and Computer Engineering, Missouri University of Science and Technology, Rolla, MO 65409, USA

[2]Southern Polytechnic College of Engineering & Engineering Technology, Kennesaw State University, Marietta, GA 30060, USA

[a)] Electronic mail: ianf@kennesaw.edu

This paper investigates manganese-doped zinc oxide (ZnMnO) thin films grown using the atomic layer deposition (ALD) technique. ZnO and MnO layers were deposited alternatively using diethyl zinc (DEZn) and manganese (III) acetylacetonate ($Mn(acac)_3$) as metallic precursors. A suppressed growth rate for both materials was observed during the growth of ZnMnO samples, which is due to reduced adsorption of the precursor molecules on the surface of the sample. Structural characterization of the ZnMnO films shows a weak polycrystalline structure for the as-deposited thin films. On the other hand, thermally annealed samples demonstrated a textured polycrystalline structure with a distinct (002) orientation. A red shift in the near band edge absorption was observed by increasing the Mn:Zn ratio. The results of this work demonstrate the potential in ALD growth of high-quality wide bandgap ZnMnO thin films that can be used as active semiconductor material in memory and logic devices.

I. INTRODUCTION

Zinc oxide (ZnO) with a wide direct bandgap energy of 3.30 eV has been extensively investigated as a II-VI compound semiconductor in different thermoelectric, piezoelectric, energy harvesting and magnetic applications.[1] ZnO has been commonly used as the top transparent electrode in optoelectronic devices due to high transparency of more than 75% in the visible region and a lower refractive index compared to other compound semiconductors.[2] The earth abundancy and non-toxicity of ZnO, in addition to its resilience to decomposition and oxidation in ambient environments, give it immense potential for use in environmentally friendly and highly efficient energy-harvesting applications.[3] Doping ZnO with transition metal (TM) elements such as Mn, Cd, and Co has shown to be effective in tailoring the electrical, optical, and magnetic properties of these thin films. This includes changes in the electrical conductivity, and the near band-edge absorption, and introduction of room-temperature ferromagnetism.[4-6] These changes have shown to be associated with the formation of TM-related clusters in the ZnO, in which they appear as mid-gap energy states in the material's energy band structure.[7,8] Growth and characterization of these semiconductor materials play an important role in fabrication of devices in which both memory and logic operations are integrated in a single device.

In this paper, the process for growth of Mn-doped ZnO (ZnMnO) thin films using atomic layer deposition (ALD) is systematically studied. The ALD growth process consists of a self-limiting and sequential chain of chemical reactions at the substrate temperatures of less than 300 °C, which leads to the formation of homogenous monolayers of the film on the substrate. This can be achieved by optimizing the growth conditions for ZnO and MnO layers, and subsequently, depositing the ZnMnO films.

The ALD growth process of the ternary ZnMnO compounds typically involves deposition of small fractions of TM-oxide and ZnO in each supercycle, and subsequently, using a high number of supercycles to complete the growth of the thin film.[9] However, increasing the total number of supercycles may further inhibit the growth of binary compounds and lead to a reduced incorporation of the dopants. This is primarily attributed to the reduced adsorption of Zn (or Mn) precursor molecules on the surface of the previously deposited MnO (or ZnO).[10] Moreover, the possibility of negative growth rates by pulsing the TM precursor, which contains CH_3 groups, may lead to complications in the structural properties of the deposited thin film,[11] and could add to the puzzling optical, electrical, and magnetic properties of these thin films. In this paper, we concentrate on the low-temperature ALD growth of ZnMnO thin films that are deposited with a fewer number of supercycles. The effect of suppression in growth rate of MnO and ZnO bilayers and is investigated. Moreover, the structural properties of the as-deposited and thermally annealed samples are characterized in order to study the effect of Mn-dopant incorporation in the ZnMnO samples.

II. EXPERIMENTAL

ZnMnO, ZnO, and MnO thin films are deposited using the GemStar XT thermal ALD system on *n*-type phosphorous-doped (100) silicon substrates with the carrier concentration of ~5×10^{14} cm^{-3} and resistivity of ~9 Ω.cm, and at varying growth conditions, including the growth temperature, precursor pulsing time, and Zn:Mn ratio. The precursor purging time is also varied to study its effect on the growth rate of the thin films, considering a viscous gas flow regime in the ALD growth process.[12] Diethyl zinc (DEZn) and manganese (III) acetylacetonate ($Mn(acac)_3$) are used as the metallic sources

for zinc and manganese, alongside DI H_2O as the oxidant. High-purity nitrogen (99.9999%) was used as the carrier gas with a flow rate of 40 sccm. Further details regarding the growth process is shown in Table I. A working chamber pressure of ~1 Torr was maintained at this nitrogen gas flow rate using a multi-stage dry mechanical pump with a pumping speed of 16 L/s. It should also be noted that the samples were placed in the same location on the sample holder inside the chamber in order to avoid any potentially unwanted variation in the uniformity of the deposited thin films.

Table I. Summary of ALD growth parameters for ZnO and MnO thin films.

	Parameter	Condition
Zinc		Diethylzinc
	Bubbler (precursor) temperature	~25 ℃
	Pulse time	100, 200, 400 ms
	Purge time	4, 6, 28 s
Manganese		Manganese (III) acetylacetonate
	Bubbler (precursor) temperature	92, 130, 160 ℃
	Pulse time	1150, 2000, 3000, 4000 ms
	Purge time	6, 28, 50 s
Growth (substrate) temperature		200 ℃
Manifolds temperature		170 ℃
Working Chamber pressure		1 Torr

It has been shown that the use of $Mn(acac)_3$ could partly be responsible for reducing the formation of foreign phases of Mn oxides, such as MnO_2 and Mn_3O_4, as compared to the other commonly used Mn precursors, such as tris(2,4-pentanedionato)

manganese (III) ($Mn(thd)_3$) or bis(ethylcyclopentadienyl) ($Mn(EtCp)_2$).[13,14] Also, reducing the processing temperature to less than 200 °C has shown to be helpful in preventing the formation of these secondary phases, which will result into a more uniform and higher quality ALD-grown ZnMnO thin films.[15]

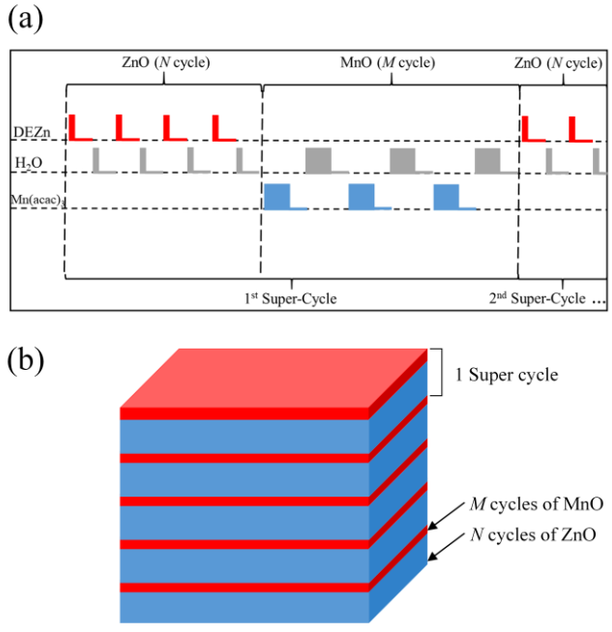

FIG. 1. Schematic diagram of (a) cycle sequences for ALD growth of ZnMnO, (b) each supercycle consists of *N* cycles of ZnO and *M* cycles of MnO.

Figure 1 shows the schematics of the sequential growth of ZnMnO thin films, where one supercycle includes *N* cycles of ZnO and *M* cycles of MnO monolayer growth. The total thickness and the growth per-cycle (GPC) of the films were determined by ex-situ spectroscopic measurements using a J.A. Woollam ellipsometer at an incident angle of 75° and a wavelength range of 300–1000 nm. Details regarding the designed model used for fitting the experimental ellipsometry data can be found elsewhere.[16] The near-

surface compositional analysis of the samples was performed by means of X-ray photoemission spectroscopy (XPS) using Al-Kα X-ray radiation source. The acquired spectra were analyzed using CasaXPS software and calibrated based on C 1*s* spectrum at 284.8 eV as the reference to remove the effect of charging.[17]

Moreover, the effect of thermal annealing on the crystalline structure of the ALD-grown ZnMnO thin films is investigated, since either an amorphous or weak crystalline structure for the as-grown ZnO has been reported.[18] Post-growth annealing has shown to improve the diffusion of Mn dopants into the film.[19] However, it should be noted that high-temperature annealing of the ZnMnO samples might contribute to formation of other Mn-oxide phases, such as Mn_2O_3., as well as spinodal decomposition of the grown films if the samples were kept at an elevated temperature for an extended period of time.[20] Spinodal decomposition of ZnMnO thin films has shown to be caused by strong attractive interactions between the Mn impurity clusters within the thin film, which leads to large inhomogeneity in Mn distribution and unpredictable variation in magnetic and optical properties of the thin films.[15,21]

The samples were annealed using a MILA-5000 mini-lamp rapid thermal annealing system at a temperature of 800 ℃ for 1 hr in a nitrogen environment.[22] The rapid thermal annealing under these conditions was not expected to result in significant spinodal decomposition of these samples and none was observed. The crystalline structure of the annealed ZnMnO thin films was investigated using high-resolution X-ray diffraction (XRD) measurements with Cu Kα X-ray source (1.54056 Å). The room temperature photoluminescence (PL) spectra were acquired using an Edinburgh Instruments FS5 system with an excitation wavelength of 325 nm. Surface morphology

of the thin films was studied using a Veeco Nanoscope atomic force microscopy (AFM) system by performing 2 μm × 2 μm scans.

III. RESULTS AND DISCUSSION

A. Growth of ZnO thin films by ALD

ZnO thin films were grown on the *n*-type phosphorous-doped (100) silicon substrate. A total of 315 cycles were completed during each growth set. Initial growth conditions included a DEZn and H_2O pulse of 100 ms and purge of 28 s at the growth temperature of 200 ℃. It should be noted that variation in thickness of the samples could possibly occur if the samples are located at distance from each other in the chamber.[23] Therefore, in this study, the samples were kept at similar location in the chamber to avoid unintentional variation in their thickness. A gradient of less than 1 nm was observed in the measured thickness of the samples that were deposited under similar growth conditions over 6" diameter platter.

Figure 2 shows the changes in the GPC of ZnO films with variation in the DEZn pulse time. A significant increase in the GPC from 0.68 to 1.50 Å/cycle was observed by increasing the DEZn pulse time from 100 to 200 ms, as shown in Figure 2. This shows the existence of unsaturated areas on the surface of the substrate in the case of shorter pulse times. In other words, the existence of unreacted hydroxyl groups on the surface of the substrate results in smaller growth rates.[24] However, increasing the pulse time from 200 to 400 ms does not noticeably increase the GPC. This indicates that the surface of the substrate has reached to a saturation in adsorbing the DEZn precursor molecules and confirms the self-limiting nature of the ALD growth behavior.

It is notable that decreasing the growth temperature from 200 ℃ to 150 ℃ has been shown to slightly reduce the GPC to 1.41 Å/cycle for DEZn pulse time of 200 ms, as shown in Figure 3.a. However, a larger variation in the GPC has been observed for growth temperatures outside of the designated window that is used in this work.[25,26] An increase in the near band edge emission intensity is observed for the samples grown at 200 ℃ compared to that of the samples grown at 150 ℃, as shown in Figure 3.b. On the other hand, a decrease in the intensity of the broad green-yellow-red PL emission is observed for the samples grown at higher temperature, which is likely due to reduction in density of the deep level defects, such as zinc vacancies or oxygen antisites.[27-29]

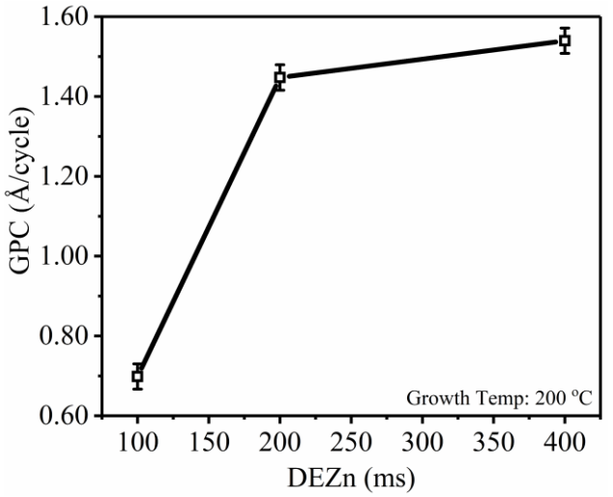

FIG. 2. Effect of change in the DEZn pulse time on the GPC of ALD-ZnO films.

Moreover, improved crystalline structure is expected by increasing the growth temperature. High resolution transmission electronic microscopy (HRTEM) image, shown in Figure 4, demonstrates a weak polycrystalline structure for the samples grown

at 200 °C, where randomly oriented ZnO grains are surrounded by amorphous ZnO pockets.[30]

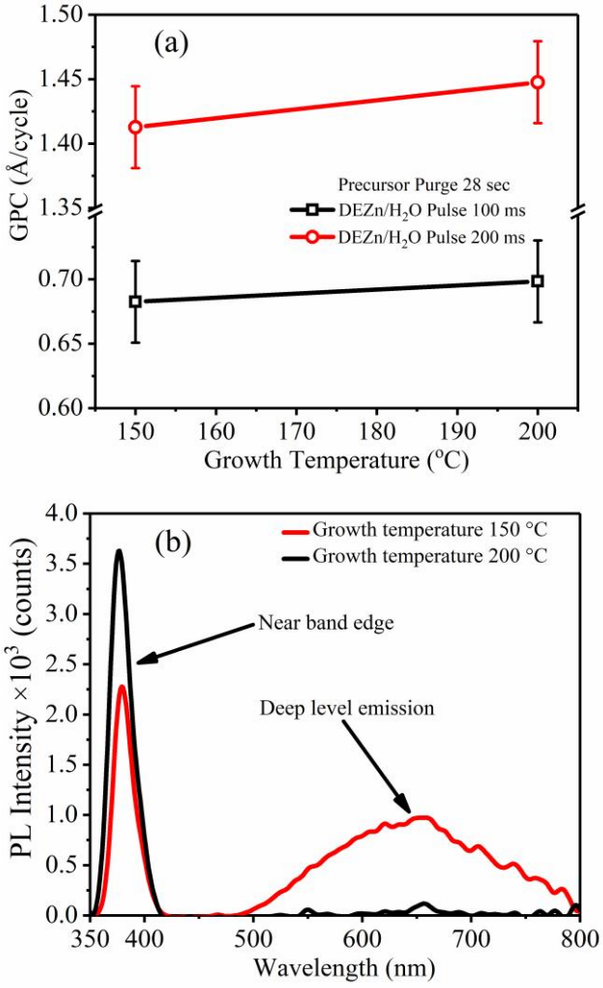

FIG. 3. (a) Effect of growth temperature on the GPC of ALD-ZnO films, and (b) acquired PL spectrum for the samples grown at different temperatures.

Decreasing the purge time from 28 to 4 s has led to an increase in the GPC from 1.50 to 1.60 Å/cycle. This can be related to the changes in the surface chemistry of the substrate for longer purging times that could lead to a reduction in the number of active monoethyl zinc sites. DEZn pulse and purge times of 200 ms and 4 s at a substrate temperature of 200 °C were used to reach to an estimated GPC of 1.60 Å/cycle during the

growth of the ZnMnO thin films, which is similar to what has been reported elsewhere.[18,21] This is about 50–60% of a complete monolayer growth of ZnO, depending on the interplanar distances of ZnO planes (2.48~2.82 Å).[24,31]

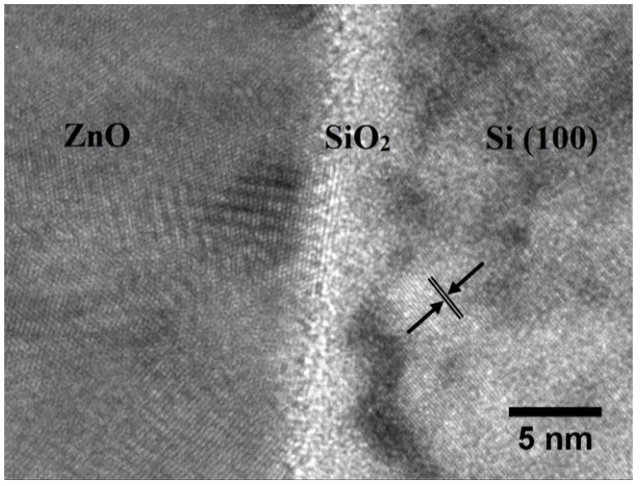

FIG. 4. High resolution TEM image (HRTEM) of the as-grown ZnO thin films on (100) Si substrate (growth temperature = 200 ℃).

B. Growth of MnO thin films by ALD

The ALD growth of MnO thin films was studied by completing 94 cycles at the substrate temperature of 200 ℃ and varying the $Mn(acac)_3$ pulse and purge times as well as the precursor temperature. A heating jacket was used around the bubbler to increase the precursor temperature. A maximum growth rate of 0.48 Å/cycle was observed at the precursor temperature of 130 ℃. However, the GPC decreases to 0.27 Å/cycle by increasing the precursor temperature to 160 ℃, which can be explained by considering the decomposition temperature of the $Mn(acac)_3$ precursor at about 159~161 ℃.[32] Similarly, a further decrease in the GPC to 0.22 Å/cycle was observed by increasing the

growth temperature from 200 to 260 °C, which can be related to the decomposition of the precursor at higher temperatures and formation of a CVD-like growth process.

The highest GPC was observed for the $Mn(acac)_3$ pulse time of 1150 ms. Typically, longer purge times of more than 45 s have been used in the ALD growth of MnO thin films using $Mn(CpEt)_2$ as the metallic precursor.[33,34] However, we only observed a slight decrease in the GPC from 0.28 to 0.24 Å/cycle by increasing the purge time from 6 s to 50 s. Nonetheless, it should be mentioned that the equivalent GPC of MnO films grown using $Mn(acac)_3$ in this work was found to be within the range of the reported values using $Mn(EtCp)_2$ and $Mn(thd)_3$ precursors.[35,36] $Mn(acac)_3$ Pulse and purge times of 1150 ms and 6 s at the substrate temperature of 200 °C were used to grow the MnO layers (GPC ~0.48 Å/cycle) in ZnMnO thin films.

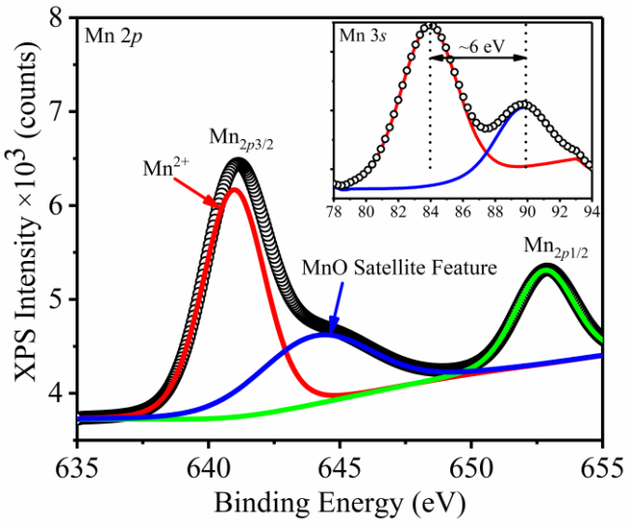

FIG. 5. Mn 2*p* XPS spectra of ALD-MnO thin films (growth temperature 200 °C, $Mn(acac)_3$ pulse time:1150 ms, purge time: 6 s). Inset shows the Mn 3*s* XPS spectra.

The XPS 2*p* spectra of the ALD-MnO layers ($Mn(acac)_3$ pulse time: 1150 ms, purge time: 6 s) are shown in Figure 5, where a satellite feature with a binding energy around 645 eV is also observed. This has been only seen for MnO films and is not present for MnO_2 or Mn_2O_3.[37] Moreover, the inset in Figure 5 shows the XPS 3*s* spectra with two split-peak elements caused by electron exchange between the 3*s* and 3*d* orbitals. The width of the peak splitting indicates exchange interaction energy that can be used for approximating the phase of the material.[38] Here, the measured splitting width of 6 eV falls within the range for what has been reported for MnO.[39]

C. Growth of ZnMnO thin films by ALD

One supercycle in the ZnMnO ALD growth consists of *N* cycles of ZnO and *M* cycles of MnO, as shown in Figure 1. A total of four samples with varying Zn:Mn cycle ratio were grown using this technique, as shown in Table II, to reach an estimated thickness of ~45 nm. The *M* number of MnO cycles was kept at 94, which is mainly due to very small growth rate. However, the number of ZnO cycles and total number of supercycles were varied to reach an estimated total thickness of 45–50 nm. The ellipsometry measurements were performed after the growth to measure the true thickness of the samples. Figure 6 shows the AFM images of the as-grown samples. The root-mean-square (RMS) surface roughness values of the samples were measured to be between 1.5 and 2.5 nm, except for Sample B, in which an RMS roughness of 4.9 nm was calculated. However, it should be noted that the surface morphology of the ALD-grown thin films is much smoother than those deposited by other growth techniques.[40-42]

Table II. Summary of ALD growth parameters for ZnO and MnO thin films.

Sample	ZnO cycles (*N*)	MnO cycles (*M*)	Supercycles	Measured thickness (nm)
A	250	94	1	43
B	125		2	39
C	73		3	31
D	34		4	21

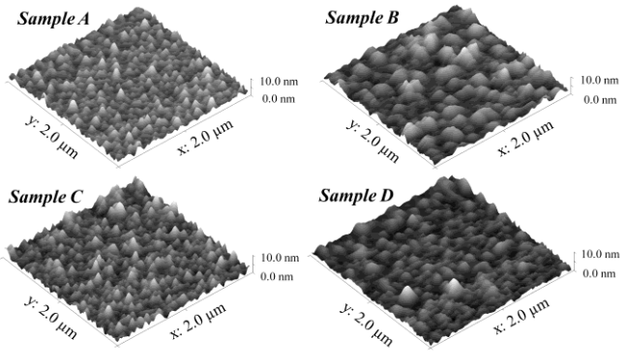

FIG. 6. AFM images of the as-grown ZnMnO samples measured by the AFM.

It should be noted that the measured thickness of the ZnMnO samples was less than the initial estimation. This could be related to the smaller GPC of ZnO and MnO layers during the ZnMnO thin film growth compared to the GPC that was calculated for pure ZnO and pure MnO thin films. Figure 7 shows the sequential ALD growth of the ZnMnO thin films. It could be inferred that the first *N* cycles of ZnO on the Si substrate would grow with approximately the same growth rate of ~1.6 Å/cycle that was calculated for pure ZnO (Figure 7.a). However, the subsequent growth of MnO could possibly have a lower-than-expected growth rate due to deposition on the ZnO surface. Similar

observations have been reported for ALD growth of (Al,Ti)-doped ZnO thin films, in which lower-than-expected growth rates were observed for ZnO, Al_2O_3, and TiO_2 layers due to longer incubation time of the materials.[9,43]

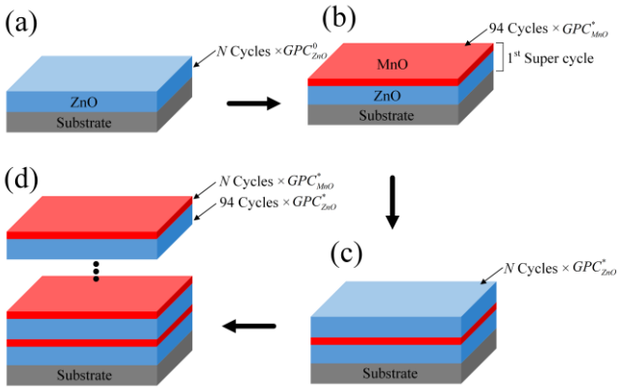

FIG. 7. Representative schematics of sequential ALD growth of ZnMnO samples by (a)-(d) depositing alternative layers of ZnO and MnO.

For example, in Sample A, an approximate thickness of ~40 nm is expected for the 250 cycles of ZnO grown directly on the substrate (GPC^0_{ZnO} =1.6 Å/cycle). This would result to an estimated GPC of 0.3 Å/cycle for the MnO layers grown on ZnO surface, as depicted in Figure 7.b. Similarly, during the growth of *N* cycles of ZnO in the second supercycle (Figure 7.c), a decrease in the GPC of ZnO is possible due to reduction in adsorption of the DEZn molecules on the MnO surface. Ye et al. and Banerjee et al. have modelled the suppressed growth of ZnO films on TiO_2 and MnO layers by considering an exponential behavior.[9,10] The suppressed growth of ZnO layers in the ZnMnO thin films can be formulated by fitting the measured thickness values and is expressed as

$$GPC^*_{ZnO} = GPC^0_{ZnO}(1-e^{-8.7\times10^{-3}N}) \quad (1)$$

where GPC^{*}_{ZnO} represents the growth rate of the ZnO films grown on MnO layers, GPC^{0}_{ZnO} is the approximate GPC deduced for the pure ZnO (or the first *N* cycles of ZnO grown directly on substrate), and *N* is the number of ZnO cycles. This indicates that ZnO encounters a major barrier while growing on the MnO surface, which affects the total thickness of the ZnMnO film.

Existence of negative growth rates (i.e. etching) during the deposition of ZnO/MnO bilayers could likely be another possible reason for the lower-than-estimated thickness of the samples. In-situ thickness measurements performed using quartz crystal microbalance (QCM) during the ALD growth of Al_2O_3/ZnO bilayers have reportedly shown that the TMA precursor, when injected into the chamber, forms a highly exothermic reaction with the hydroxylated ZnO surface by transferring CH_3 groups from Al to Zn, and results into dissociation of Zn atoms from the surface of the sample.[11] Similar observations have been reported for the ALD growth of MgMnCoO mixed oxide films, in which the $Mg(thd)_2$ and $Mn(thd)_2$ were found to form reactions leading to dissociation of Co atoms from the surface of the sample.[35] It is likely that a similar reaction could occur, in which ethyl groups from the DEZn precursor molecules will be transferring to Mn, forming volatile $Mn(Et)_x$ species, and resulting in the possible etching of the MnO layer. As a result, a lower-than-expected total thickness of the films could be observed.

1. Structural properties

Figure 8 shows the high resolution θ–2θ XRD scans of the ZnMnO samples grown on *n*-Si substrate and annealed at 800 °C for 1 hr. The XRD characterization showed a weak polycrystalline structure with no distinguishable diffraction peak for the

as-grown ZnMnO samples. On the other hand, the thermally annealed samples demonstrated a highly textured polycrystalline structure. The annealing process is also expected to increase the thermally driven atomic diffusion of Mn in the overall thin film structure.[44] High-temperature annealing has been shown to be a contributing factor in formation of secondary MnO_x phases. However, large scale spinodal decomposition of the thin films was not expected under these annealing conditions nor was it observed. This could potentially lead to unwanted changes in magnetic, optical, and electrical properties of the thermally annealed ZnMnO thin films.[15,21]

The occurrence of forbidden Si (200) reflection at 2θ=32.98º has been shown to be caused by multiple diffractions from the substrate.[44] The broad-intensity shoulder at the low-angle side of the Si (200) peak observed for Sample B could be attributed to slight variation in in-plane orientation of the samples placed on the stage.[45] The XRD patterns reveal only one (002) orientation, while no discrete peaks related to MnO phase were observed.[6,45] Moreover, the (002) peaks observed in the patterns reveal the *c*-axis orientation of the ZnMnO thin films, decreasing to lower angles as the ratio of MnO increases from Sample A to D. This is likely due to substitution of Mn^{2+} ions with larger ionic radii (0.91 Å) into Zn^{2+} sites (0.83 Å),[46] which results in an increase in the *c*-axis lattice constant from 5.201±0.002 Å for Sample A to 5.212±0.001 Å for Sample D.

The average crystallite (grain) size of the ZnMnO samples are estimated using the Scherrer's equation and can be expressed as

$$D_v = \frac{K\lambda}{\beta \cos(\theta)} \quad (2)$$

where D_v is the volume weighted crystallite size, K is the Scherrer constant equivalent to 0.89, λ is the wavelength of the X-ray source (1.54056 Å), and β is the FWHM of the observed (002) peak.[47]

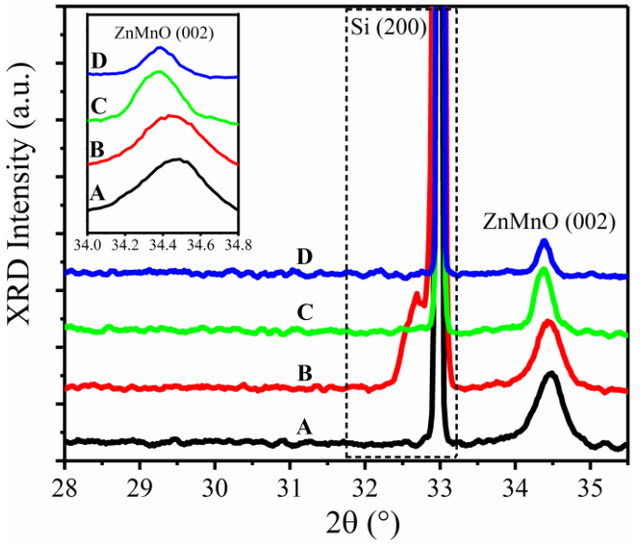

FIG. 8. XRD patterns for the ZnMnO samples grown on *n*-Si (100) substrate and annealed at 800 ℃. Inset shows the (002) reflection peak shift for the ZnMnO samples.

Table III. Structural characterization of the annealed ALD-ZnMnO samples.

Sample	Interplanar spacing, d (Å) ±0.001	Lattice constant, c (Å) ±0.001	FWHM, β (º)	Crystallite size, D_v (nm)
A	2.600	5.201	0.35	23.21
B	2.601	5.203	0.36	22.56
C	2.607	5.213	0.25	32.72
D	2.606	5.212	0.18	44.90

As shown in Table III, an increase in the crystallite size and decrease in FWHM of the (002) peak in Sample D are observed compared to that of the Sample A, which indicates an increase in crystalline quality of the ZnMnO film in Sample D. This is contrary to what has been reported elsewhere regarding the degradation in crystalline quality and higher FWHM of the (002) diffraction peak by increasing the Mn incorporation in the ZnO films.[10,48,49] However, it should be noted that in the ALD technique, due to its sequential growth process, Mn-dopants are introduced through growth of alternative MnO layers between the ZnO layers. Therefore, the improved crystalline quality observed for Sample D is presumably related to the nature of the growth technique and could also be due to higher number of supercycles used in the ALD growth process. In other words, a higher number of supercycles may lead to enhancement in diffusion of Mn into the ZnO lattice structure and substitution with Zn^{2+} ions. On the other hand, a degraded crystal quality and higher FWHM of (002) peak is expected in the ZnMnO samples with a lower number of supercycles, where the grown thin film can be described as a MnO top layer deposited on a thick ZnO bottom layer (Sample A).

2. *Optical properties*

The optical properties of the ALD-ZnMnO samples were studied by measuring their room-temperature ultraviolet-visible (UV-Vis) absorption coefficient (α) using an Antas spectrometer. Tauc plots were drawn by plotting $(\alpha h\nu)^2$ versus photon energy ($h\nu$) and assuming a direct band transition in the wurtzite structure of ZnO.[10] The optical bandgap energies, E_g, were calculated by linearly fitting the sharp increase in the absorption near the band edge and finding the intersection of the extrapolated lines with the horizontal axis, as shown in Figure 9. The estimated value of the bandgap was found

to decrease by increasing the Mn incorporation, in which E_g decreased from 3.17 eV for Sample A to 3.08 eV for Sample D.

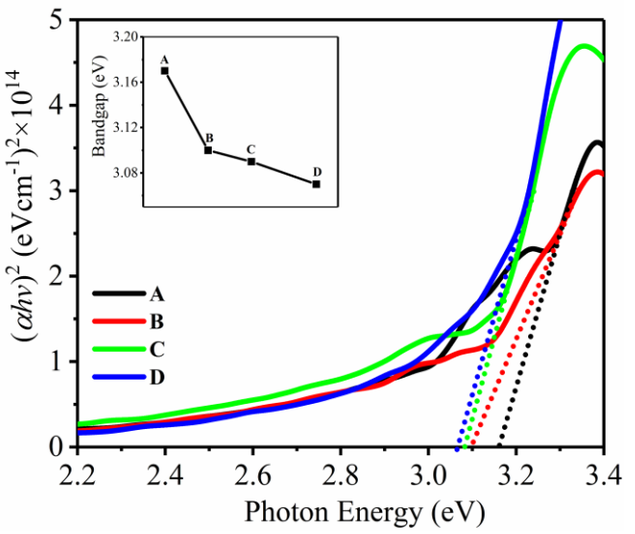

FIG. 9. Tauc plots of the ALD-ZnMnO samples acquired using room-temperature UV-Vis absorption spectroscopy.

This reduction in the bandgap energy has been attributed to the effect of band bending in the ALD-ZnMnO samples, which can be explained based on the charge transfer interaction between Mn-related impurity energy bands and the valence and/or conduction band continuum.[10,50] In order words, the intra-shell interactions between the donor and/or acceptor ionization levels of Mn^{2+} ions and the valence band holes and/or conduction band electrons lead to formation of the band bending toward lower energies in the ZnMnO samples.[51,52] Furthermore, the effect of using digital alloy structure (DA) in the growth process on tuning the optical properties of the thin films have been investigated.[53] ZnMnO DAs were grown by decreasing the thickness of each layer and increasing the total number of supercycles, and as a result, a higher Mn incorporation in

the ZnMnO thin films is expected. The Tauc plots were used to deduce the optical band gap energy of the samples, in which the lowest E_g value of 2.3 eV was calculated for ZnO:MnO (5:3)×40. However, the reasoning behind this significant shift in the bandgap energy is not clear and currently under investigation.

Figure 10 shows the acquired room-temperature PL spectra of the ALD-ZnMnO thin films, which are normalized to account for variation in the film thicknesses. Gaussian curve fitting was used to deconvolute the near band edge (NBE) PL spectrum of each sample, in which it resulted into two distinct fitting peaks that are centered at around 378 nm (~3.28 eV) and close to 400 nm (~3.09 eV). The peak at the higher energy is likely related to the NBE emission for the pure ZnO at room temperature, which can be attributed to a radiative recombination between a hole in the valence band and an electron in the conduction band.[10] On the other hand, the lower energy emission peak could be due to radiative transitions between the Mn-related energy levels and the valence and/or conduction band continuum. By increasing the total MnO cycles from Sample A to D, the lower energy peak becomes more dominant compared to the higher energy peak. This likely shows the band bending toward lower bandgap energies in the ZnMnO thin films, as it was also observed from the absorption measurements.

The existence of the asymmetric NBE emission spectrum with two deconvoluted components could be alternatively explained based on the exciton transitions in the band structure of the material, in which the higher energy emission peak is likely associated with the free exciton transitions and the lower energy emission peak is assigned to free-to-bound transitions.[54] As it can be seen in Figure 10, the lower energy peak becomes more dominant compared to the higher energy peak by increasing the total MnO cycles

from Sample A to D. This indicates an increase in the Mn-related impurity band edge bound excitons and defect-induced exciton localization, and at the same time, a reduction in free exciton transitions by increasing the Mn incorporation.[55]

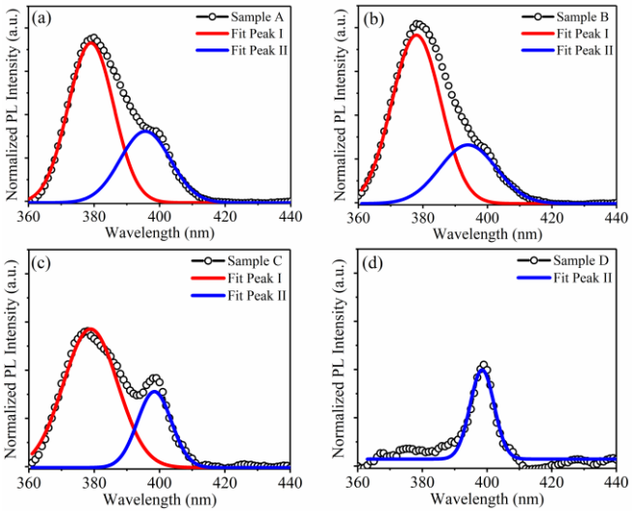

FIG. 10. Normalized near band edge PL spectra of the ALD-ZnMnO samples.

Table IV. Summary of photoluminescence properties of ALD-ZnMnO samples.

Sample	NBE emission		Red Emission (nm)	NBE/Red Emission Intensity Ratio
	Fit peak I (nm)	Fit peak II (nm)		
A	378	396	655	9.2
B	377	396	655	2.0
C	376	397	655	2.3
D	N/A	398	657	2.1

In addition to the NBE peaks, an additional red emission peak centered around 655 nm was observed in the samples, which could be related to the existence of deep

defect-related energy levels well below the conduction band.[56,57] The photoluminescence properties of ZnMnO thin films are shown in Table IV, which illustrates that by increasing the total MnO cycles, the NBE/red emission intensity ratio decreases considerably. This reduction in the intensity ratio could be due to an increase in the non-radiative recombination centers, such as Zn vacancies and Mn interstitials, as can be seen by increased red emission PL intensity in these samples.

IV. SUMMARY AND CONCLUSIONS

In conclusion, the ALD growth of ZnMnO thin films by deposition of alternative layers of ZnO and MnO was studied in this paper. Approximate growth rates of 1.6 and 0.48 Å/cycle were measured for the pure ZnO and MnO thin films under the optimized growth conditions. However, the growth rates of both materials were found to be suppressed during the sequential growth in an ALD supercycle, which is likely due to reduced adsorption of the precursor on the surface of the sample. The structural characterization of the thermally annealed samples demonstrated a polycrystalline structure with a distinct (002) diffraction peak. A reduction in the peak position and increase in the *c*-axis lattice constant were observed by increasing the MnO incorporation, which is due to the substitution of Mn^{2+} ions into Zn^{2+} sites. Moreover, the UV-Vis absorption and PL measurements demonstrated a reduction in the optical bandgap of the ZnMnO samples down to ~3.08 eV, which could be related to the formation of band bending due to impurity-related energy levels in the ZnMnO samples.

ACKNOWLEDGMENTS

This research was carried out by financial support from Columbus Photovoltaics, LLC. Authors would like to thank Dr. Corey Lerner for providing constructive feedbacks throughout the project. Authors would also like to acknowledge the technical support received throughout this work from the Material Research Center (MRC) at Missouri S&T in characterizing the ALD-grown thin films.

REFERENCES

[1]C. Zhou, A. Ghods, K. L. Yunghans, V. G. Saravade, P. V. Patel, X. Jiang, B. Kucukgok, N. Lu, and I. Ferguson, Proc. SPIE **10105**, 101051K (2017).

[2]S. J. Chang, J. L. Tou, T. J. Hsueh, K. T. Lam, S. Li, C. H. Liu, and S. P. Chang, IEEE J. Photovolt. **3**, 991 (2013).

[3]K. Matsubara, P. Fons, K. Iwata, A. Yamada, K. Sakurai, H. Tampo, and S. Niki, Thin Solid Films **431-432**, 369 (2003).

[4]B. Mari, M. Tortosa, M. Mollar, J. V. Bosca, and H. N. Cui, Opt. Mater., **32** 1423 (2010).

[5]M. Godlewski, A. W. Glodowska, E. Guziewicz, S. Yatsunenko, A. Zakrzewski, Y. Dumont, E. Chikoidze, M. R. Philips, Opt. Mater. **31**, 1768 (2009).

[6]A. K. Pradhan, D. Hunter, K. Zhang, J. B. Dadson, S. Mohanty, T. M. Williams, K. Lord, R. R. Rakhimov, U. N. Roy, Y. Cui, A. Burger, J. Zhang, D. J. Sellmyer, Appl. Surf. Sci. **252**, 1628 (2005).

[7]M. Godlewski, A. Wasiakowski, V. Y. Ivanov, A. W. Glodowska, M.Lukasiewicz, E. Guziewicz, R.Jakiela, K.Kopalko, A.Zakrzewski, Y.Dumont, Opt. Mater. **32**, 680 (2010).

[8]S. Sonoda, I. Tanaka, H. Ikeno, T. Yamamoto, F. Oba, T. Araki, Y. Yamamoto, K. Suga, Y. Nanishi, and Y. Akasaka, J. Phys. Condensed Matter. **18**, 4615 (2006).

[9]Z. Y. Ye, H. L. Lu, Y. Z. Gu, Z. Y. Xie, Y. Zhang, Q. Q. Sun, S. J. Ding, and D. W. Zhang, Nanoscale Res. Lett. **8**, 1 (2013).

[10]R. Karmakar, S. K. Neogi, A. Banerjee, and S. Bandyopadhyay, Appl. Surf. Sci., **263** 671 (2012).

[11]J. W. Elam and S. M. George, Chem. Mater. **15**, 1020 (2003).

[12]S. M. George, Chem. Rev. **110**, 111 (2010).

[13]M. I. Lukasiewicz, A. Wojcik-Glodowska, E. Guziewicz, A. Wolska, M. T. Klepka, P. Dluzewski, R. Jakieła, E. Lusakowska, K. Kopalko, W. Paszkowicz, Semicond. Sci. Technol. **27**, 074009 (2012).

[14]A. Wojcik, M. Kiecana, K. Kopalko, M. Godlewski, E. Guziewicz, S. Yatsunenko, E. Lusakowska, R. Minikayev, W. Paszkowicz, K. Swiatek, Z. Wilamowski, M. Sawicki, and T. Dietl, Acta Phys. Pol. A **108**, 915 (2005).

[15]A. Wojcik, M. Godlewski, E. Guziewicz, K. Kopalko, R. Jakiela, M. Kiecana, M. Sawicki, M. Guziewicz, M. Putkonen, L. Niinisto, Y. Dumont, and N. Kelner, Appl. Phys. Lett. **90**, 082502 (2007).

[16]A. Ghods, V. G. Saravade, C. Zhou, and I. T. Ferguson, J. Vac. Sci. Technol. A **38**, 012406 (2020).

[17]W. Lu, Y. Iwasa, Y. Qu, D. Jinno, S. Kamiyama, P. M. Peterson, and H. Ou, RSC Adv. **7**, 8090 (2017).

[18]S. J. Lim, S. Kwon, and H. Kim, Thin Solid Films **516**, 1523 (2008).

[19]A. Wojcik, K. Kopalko, M. Godlewski, E. Guziewicz, R. Jakiela, R. Minikayev, and W. Paszkowicz, Appl. Phys. Lett., **89**, 051907 (2006).

[20]D. Soundararajan, J. S. Salazar, J. M. Ko, and K. H. Kim, J. Magn., **16**, 216 (2011).

[21]M. Godlewski, A. Wokcik, K. Kopalko, V. Y. Ivanov, Z. Wilamowski, R. Jakiela, E. Guziewicz, A. Szczepanik, P. Dluzewski, E. Chikoidze, J. Barjon, Y. Dumon, M. Putkonen, L. Niinisto, and D. Tang, Acta Phys. Pol. A **112**, 261 (2007).

[22]J. Lim and C. Lee, Thin Solid Films **515**, 3335 (2007).

[23]O. Nilsen, H. Fjellvag, and A. Kjekshus, Thin Solid Films, **444**, 44 (2003).

[24]T. Weckman and K. Laasonen, J. Phys. Chem. C **120**, 21460 (2016).

[25]E. Guziewicz, I. A. Kowalik, M. Godlewski, K. Kopalko, V. Osinniy, A. Wojcik, S. Yatsunenko, E. Lusakowska, W. Paszkowicz, and M. Guziewicz, J. Appl. Phys. **103**, 033515 (2008).

[26]D. Kim, H. Kang, J. M. Kim, and H. Kim, Appl. Surf. Sci. **257**, 3776 (2011).

[27]N. Y. YuaN, S. Y. Wang, C. B. Tan, X. Q. Wang, G. G. Chen, and J. N. Ding, J. Cryst. Growth **366**, 43 (2013).

[28]T. A. Krajewski, P. Terziyska, G. Luka, E. Lusakowska, R. Jakiela, E. S. Vlakhov, and E. Guziewicz, J. Alloy. Comp., **727**, 902 (2017).

[29]H. C. Ong and G. T. Du, J. Cryst. Growth **265**, 471 (2004).

[30]K. Tapily, D. Gu, H. Baumgart, G. Namkoong, D. Stegall, and A. A. Elmustafa, Semicond. Sci. Technol. **26**, 115005 (2011).

[31]E. B. Yousfi, J. Fouache, and D. Lincot, Appl. Surf. Sci. **153**, 223 (2000).

[32]M. A. Siddiqi, R. A. Siddiqui, and B. Atakan, Surf. Coat. Technol. **201**, 9055 (2007).

[33]B. B. Burton, F. H. Fabreguette, and S. M. George, Thin Solid Films **517**, 5658 (2009).

[34]K. L. Pickrahn,Y. Gorlin, L. C. Seitz, A. Garg, D. Nordlund, T. F. Jaramillo, and S. F. Bent, Phys. Chem. Chem. Phys. **17**, 14003 (2015).

[35]H. L. Lu, G. Scarel, X. L. Li, M. Fanciulli, J. Cryst. Growth **310**, 5464 (2008).

[36]Nilsen, H. Fjellvag, and A. Kjekshus, Thin Solid Films **444**, 44 (2003).

[37]M. C. Biesinger, B. P. Payne, A. P. Grosvenor, L. W. M. Lau, A. R. Gerson, R. St. C. Smart, Appl. Surf. Sci. **257**, 2717 (2011).

[38]M. Chigane and M. Ishikawa, J. Electrochem. Soc. **147**, 2246 (2000).

[39]B. Djurfors, J. N. Broughton, M. J. Brett, and D. G. Ivey, Acta Materialia **53**, 957 (2005).

[40]H. Chen, J. Ding, and S. Ma, Superlattice Microst., **49**, 176 (2011).

[41]K. Ogata, T. Kawanishi, K. Sakurai, S. W. Kim, K. Maejima, Sz. Fujita, and Sg. Fujita, Phys. Stat. Sol. **229**, 915 (2002).

[42]J. Ye, S. Gu, S. Zhu, T. Chen, L. Hu, F. Qin, R. Zhang, Y. Shi, Y. Zheng, J. Cryst. Growth **243**, 151 (2002).

[43]D. J. Lee, H. M. Kim, J. Y. Kwon, H. Choi, S. H. Kim and K. B. Kim, Adv. Funct. Mater. **21**, 448 (2011).

[44]Y. Wu, A. D. Giddings, M. A. Verheijen, B. Macco, T. J. Prosa, D. J. Larson, F. Roozeboom, and W. M. M. Kessels, Chem. Mater. **30**, 1209 (2018).

[45]P. Zaumseil, J. Appl. Cryst. **48**, 528 (2015).

[46]R. A. Flinn and P. K. Trojan, "Engineering Materials and Their Applications", 3rd ed. (Houghton Mifflin, Boston, 1975), p.1; The ionic radii are based on the calculations of V. M. Goldschmidt.

[47]S. M. Salaken, E. Farzana, and J. Podder, J. Semicond. **34**, 073003 (2013).

[48]S. W. Jung, S. J. An, G. C. Yi, C. U. Jung, S. I. Lee, and S. Cho, Appl. Phys. Lett., **80**, 4561 (2002).

[49]P. Singh, A. Kaushal, and D. Kaur, J. Alloy Comp. **471**, 11-15 (2009).

[50]T. Fukumura, Z. Jin, A. Ohtomo, H. Koinuma, and M. Kawasaki, Appl. Phys. Lett. **75**, 3366 (1999).

[51]T. Mizokawa, T. Nambu, A. Fujimori, T. Fukumura, and M. Kawasaki, Phys. Rev. B **65**, 085209 (2002).

[52]T. Mizokawa and A. Fujimori, Phys. Rev. B **48**, 1450 (1993).

[53]W. Sun, C. K. Tan, and N. Tansu, Sci. Rep. **7**, 1 (2017).

[54]E. Przezdziecka, E. Guziewicz, D. Jarosz, D. Snigurenko, A. Sulich, P. Sybilski, R. Jakiela, and W. Paszkowicz, J. Appl. Phys. **127**, 075104 (2020).

[55]X. Y. Meng, Y. H. Zhang, and W. Z. Shen, Phys. B Condensed Matter **404**, 1222 (2009).

[56]T. A. Hua, M. Z. Xia, H. Y. Nan, D. X. Long, Chinese Phys. B **27**, 117802 (2018).

[57]C. Pholnak, C. Sirisathitkul, D. J. Harding, and S. Suwanboon, J. Ceramic Soc. Jpn., **119**, 535 (2011).

(a)

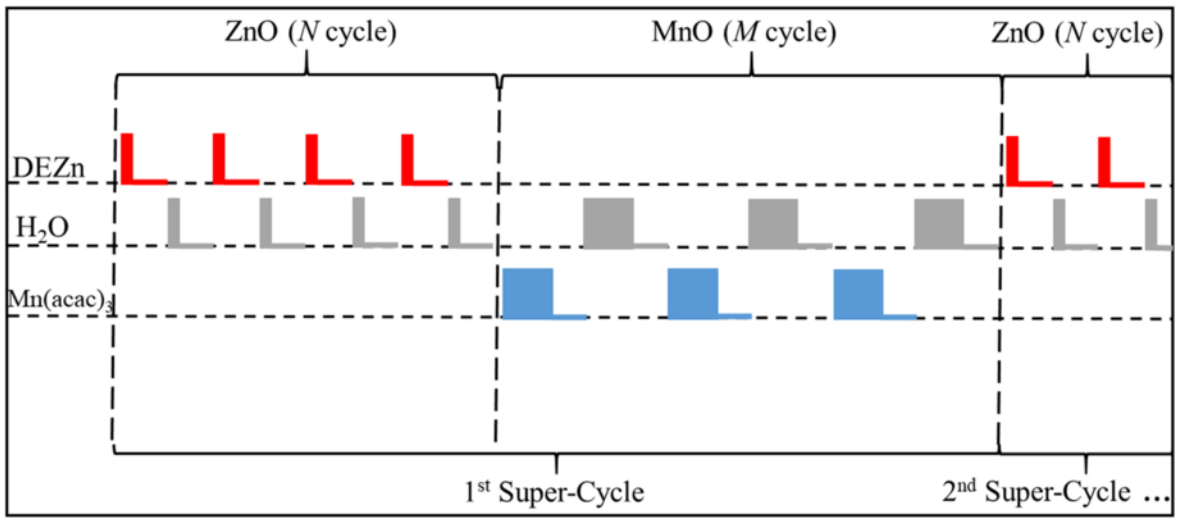

(b)

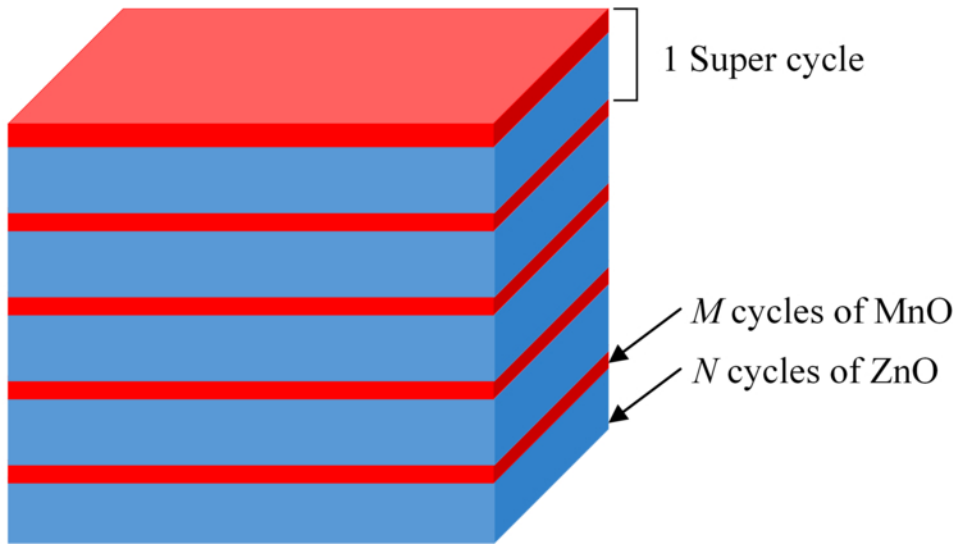

Journal of Vacuum Science Technology A

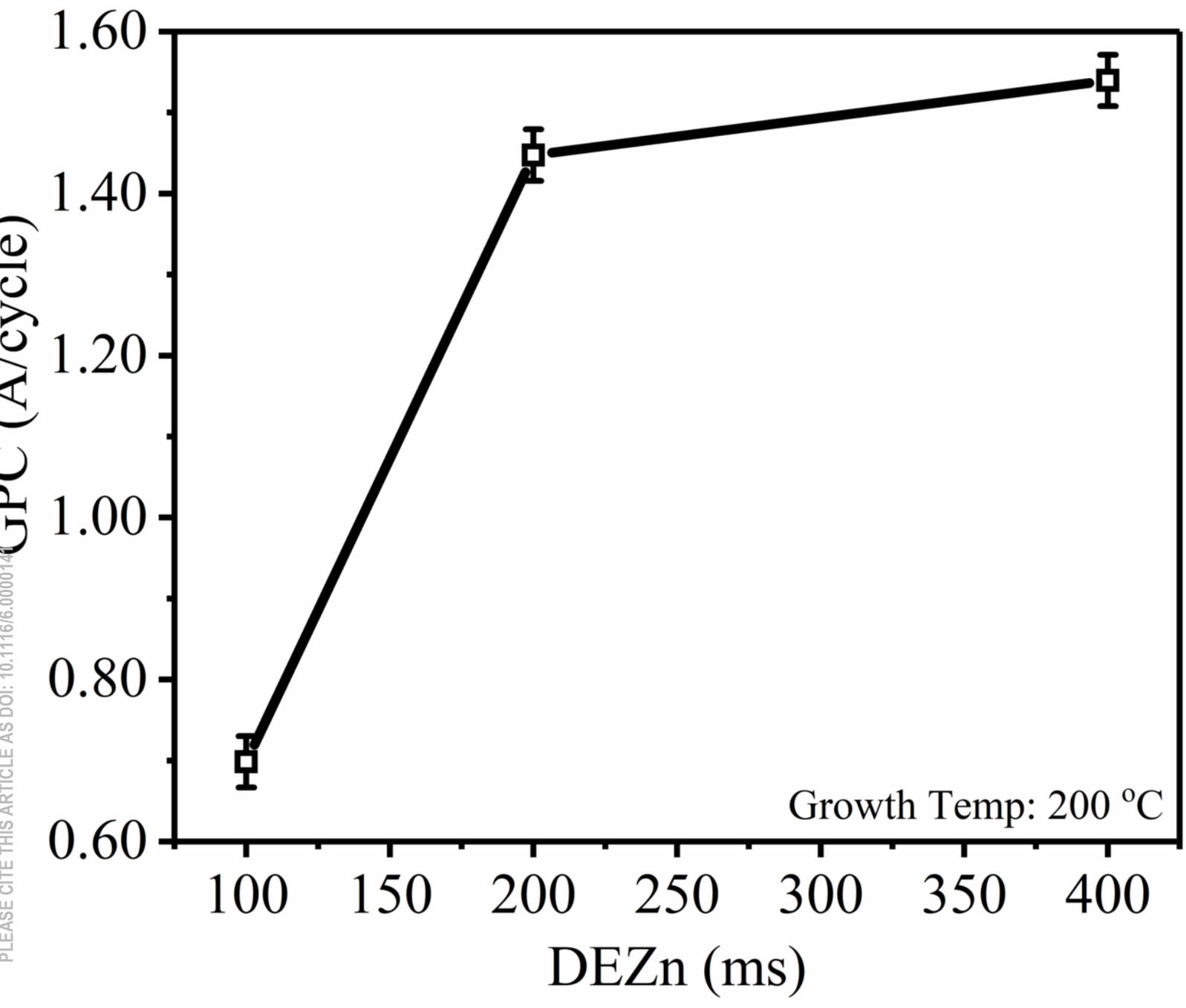

Journal of Vacuum Science Technology A

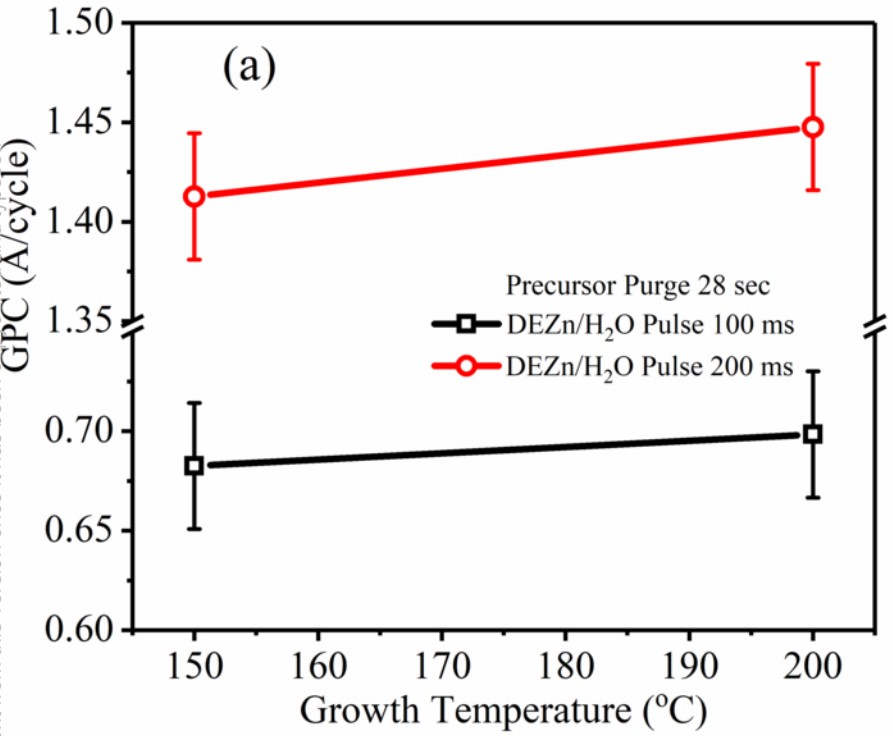

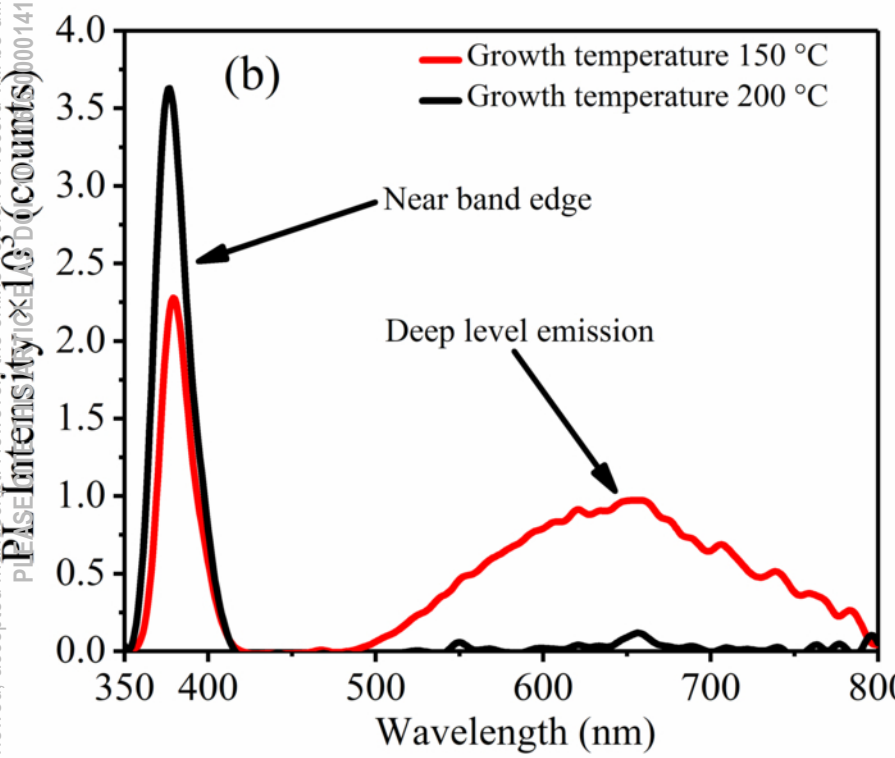

Journal of Vacuum Science Technology A

PLEASE CITE THIS ARTICLE AS DOI: 10.1116/6.0000141

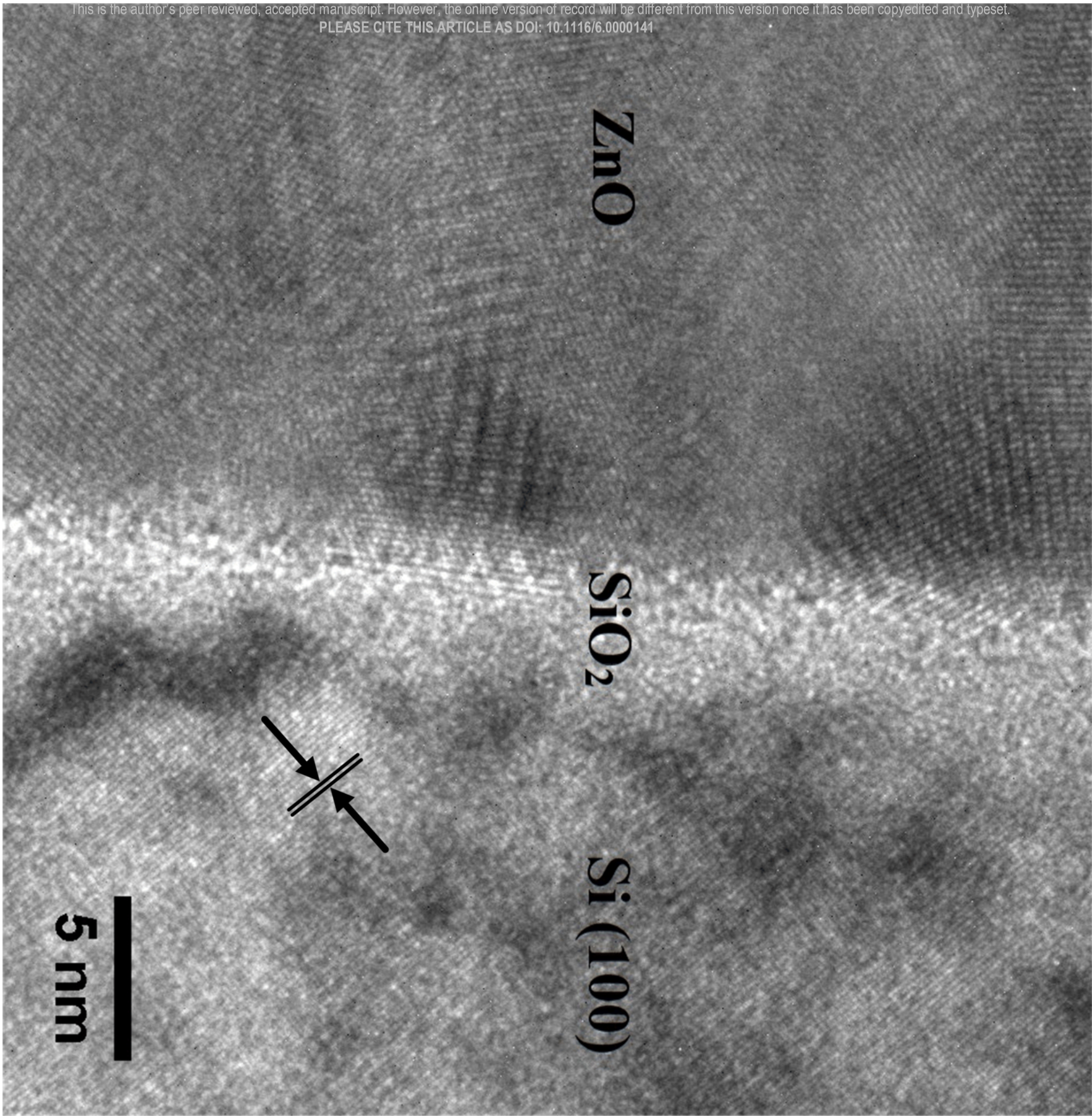

Journal of Vacuum Science Technology A

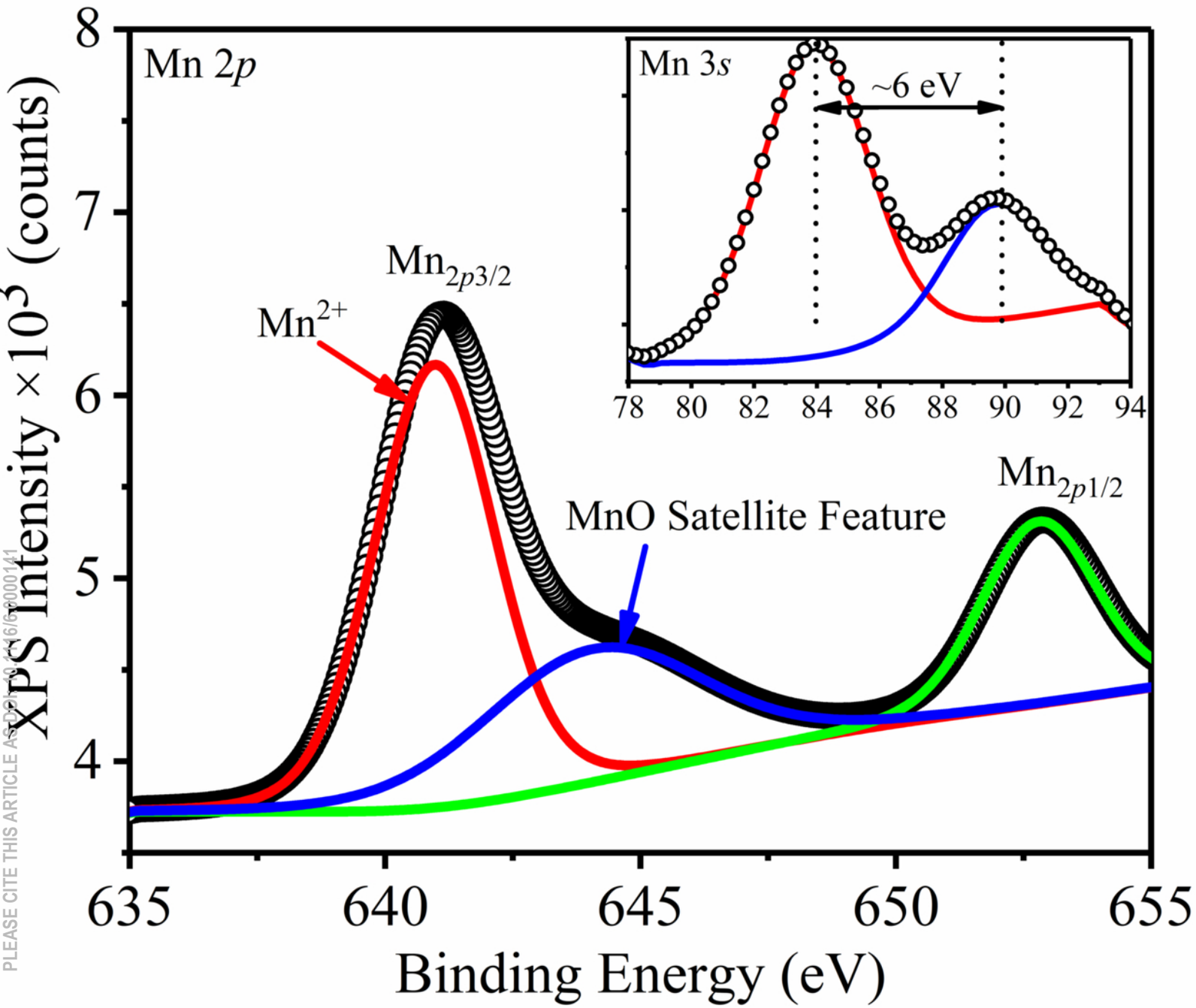

Journal of Vacuum Science Technology A

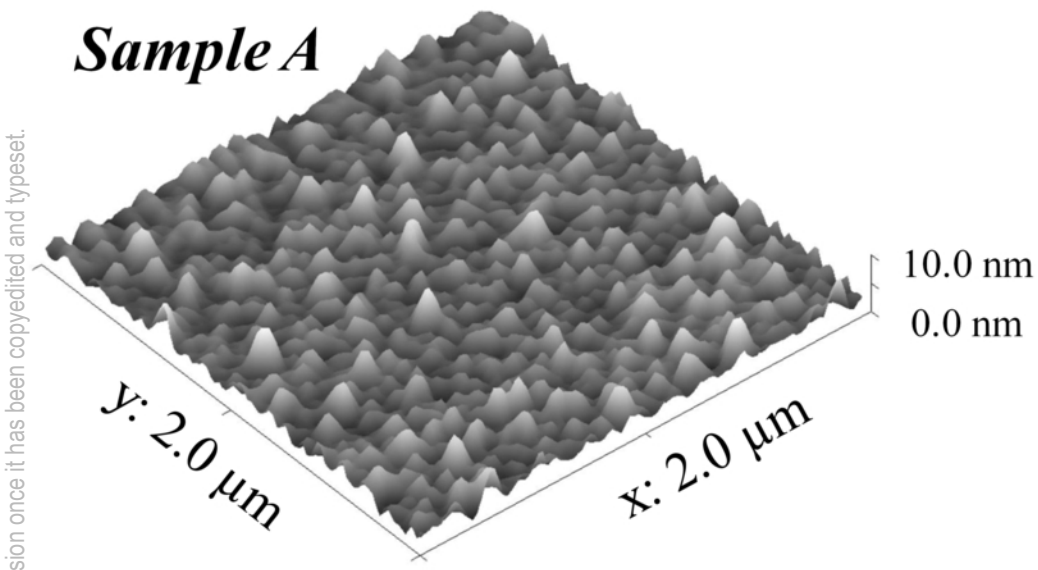

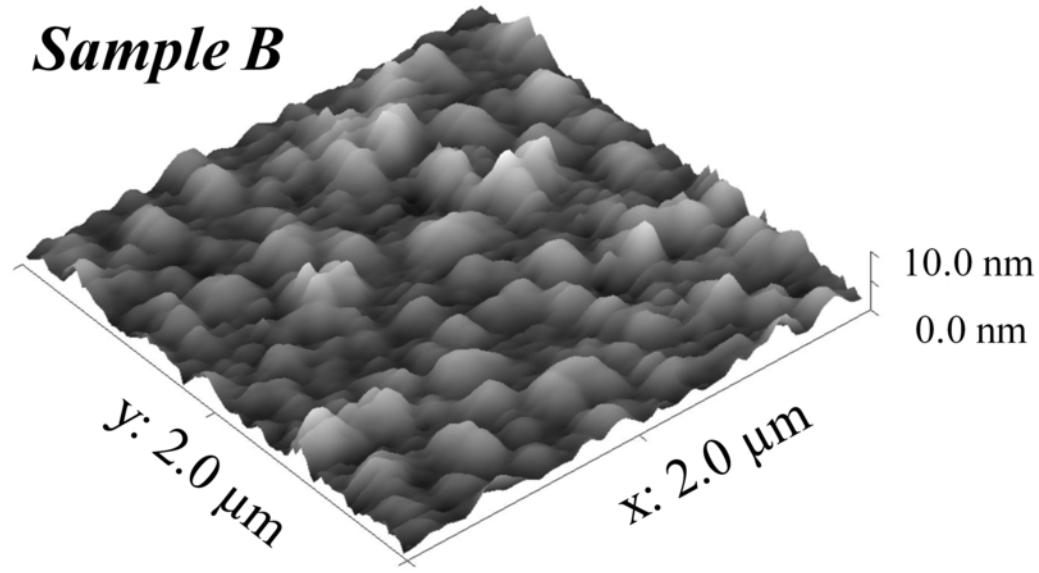

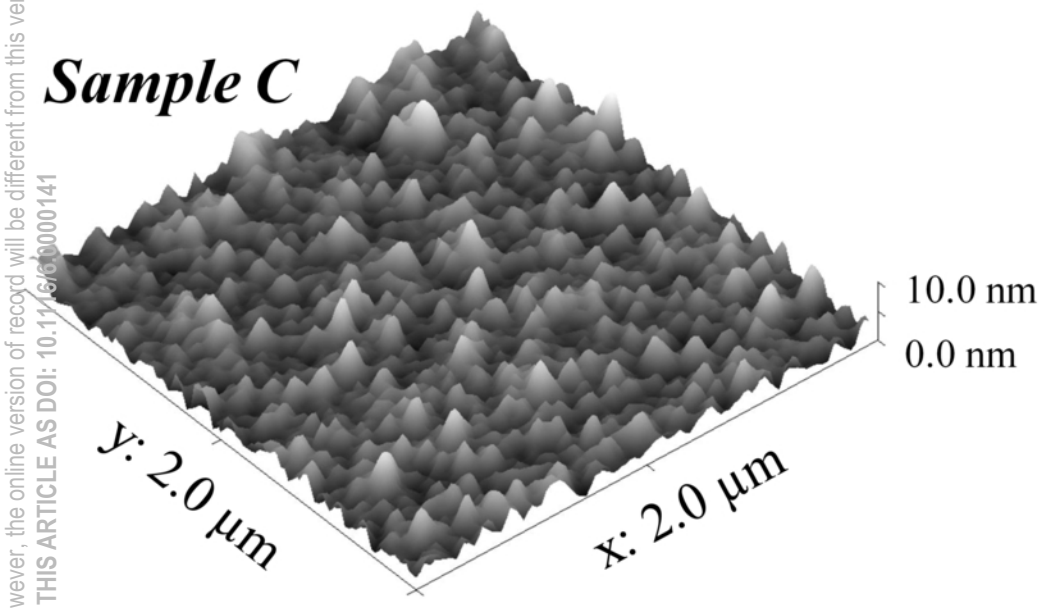

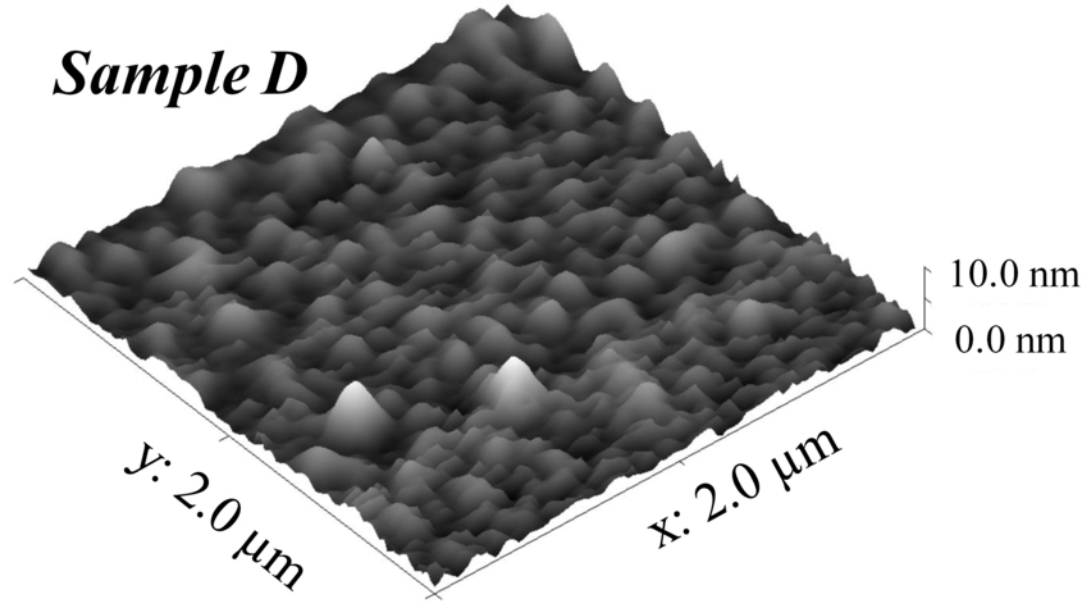

Journal of Vacuum Science Technology A

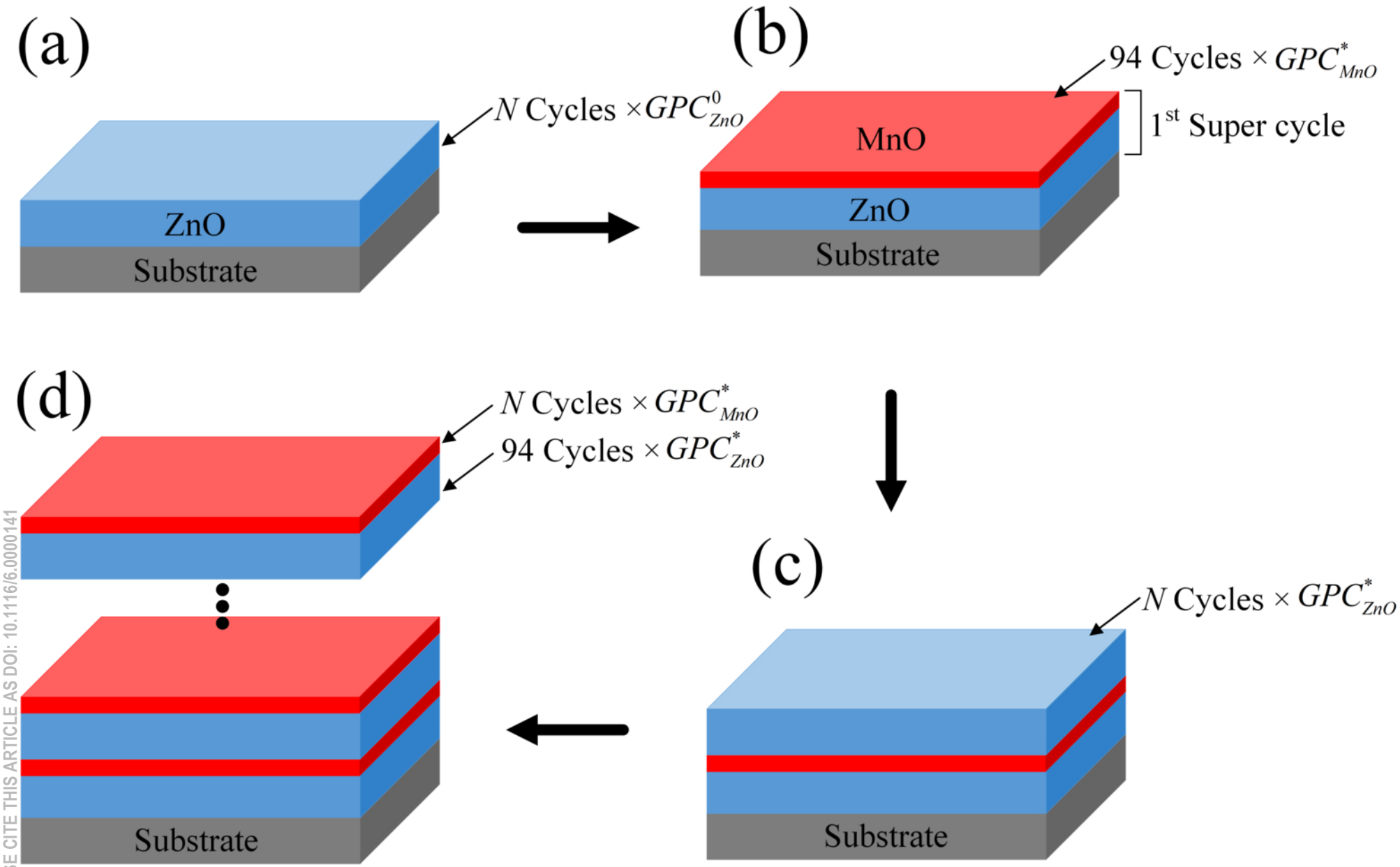

Journal of Vacuum Science Technology A

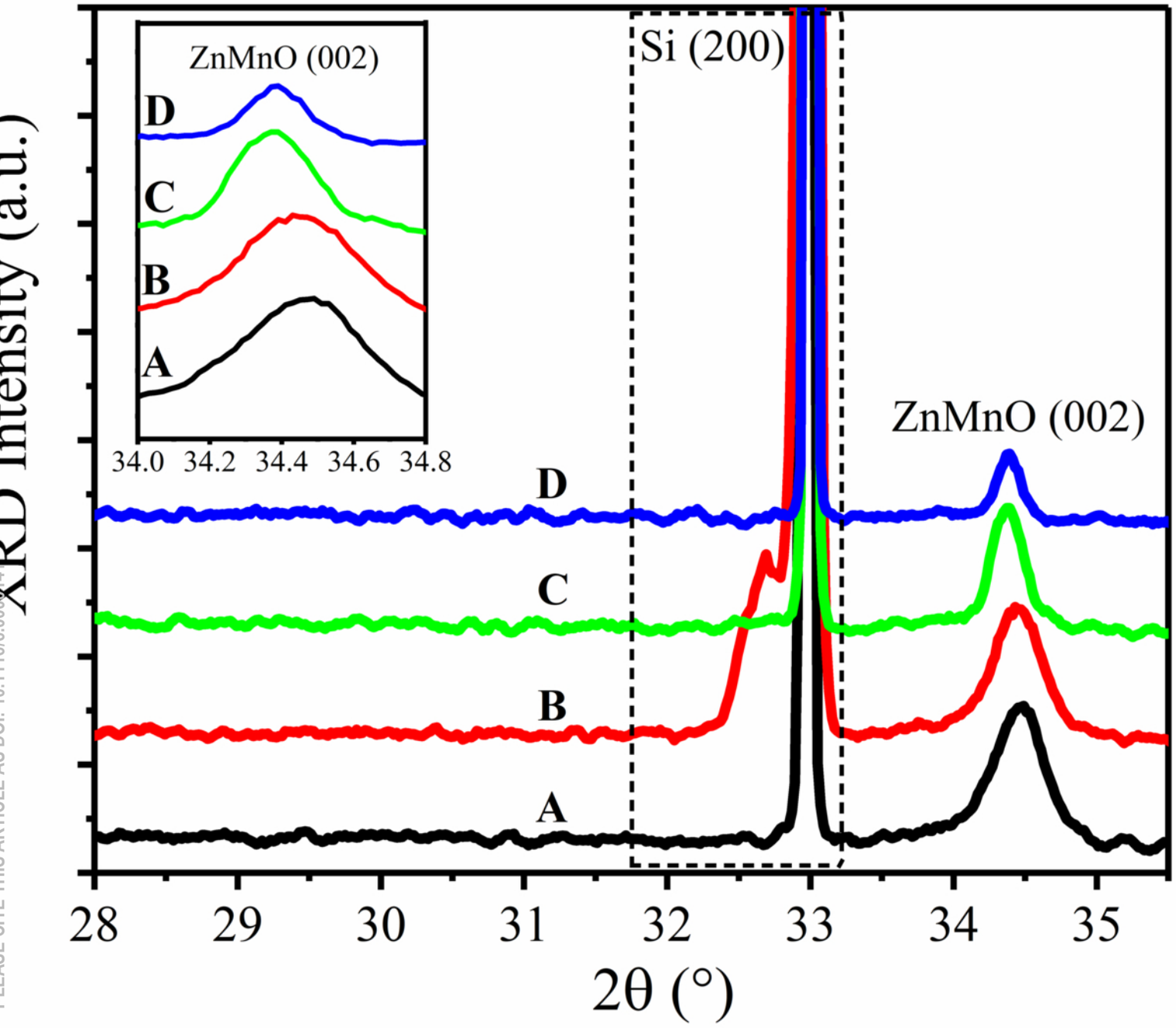

Journal of Vacuum Science Technology A

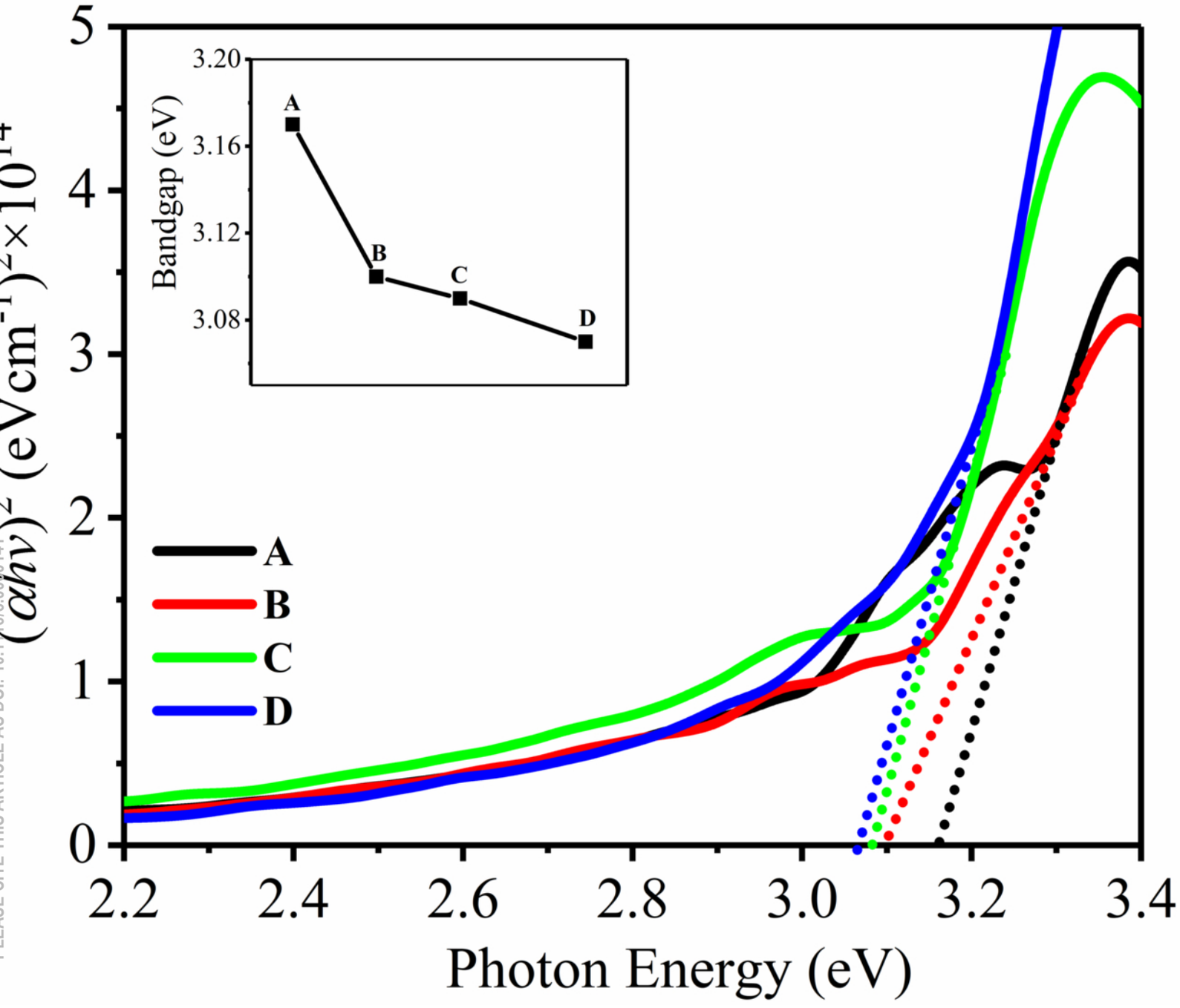

Journal of Vacuum Science Technology A